Journal of Applied Geophysics 133 (2016) 9–15

Contents lists available at ScienceDirect

Journal of Applied Geophysics

journal homepage: www.elsevier.com/locate/jappgeo

Wave equation dispersion inversion using a difference approximation to the dispersion-curve misfit gradient

Zhen-dong Zhang[a,*], Gerard Schuster[a], Yike Liu[b], Sherif M. Hanafy[a], Jing Li[a]

[a] Department of Physical Science and Engineering, King Abdullah University of Science and Technology, Thuwal 23955-6900, Saudi Arabia
[b] Institute of Geology and Geophysics, Chinese Academy of Sciences, Beijing 100029, China

ARTICLE INFO

Article history:
Received 30 January 2016
Received in revised form 7 June 2016
Accepted 20 July 2016
Available online 25 July 2016

Keywords:
Surface wave
Dispersion curve
Wave equation
Inversion

ABSTRACT

We present a surface-wave inversion method that inverts for the S-wave velocity from the Rayleigh wave dispersion curve using a difference approximation to the gradient of the misfit function. We call this wave equation inversion of skeletonized surface waves because the skeletonized dispersion curve for the fundamental-mode Rayleigh wave is inverted using finite-difference solutions to the multi-dimensional elastic wave equation. The best match between the predicted and observed dispersion curves provides the optimal S-wave velocity model. Our method can invert for lateral velocity variations and also can mitigate the local minimum problem in full waveform inversion with a reasonable computation cost for simple models. Results with synthetic and field data illustrate the benefits and limitations of this method.

© 2016 Elsevier B.V. All rights reserved.

1. Introduction

Conventional surface wave inversion methods can be separated into two categories: 1) 1D inversion for a layered medium using semi-analytical solutions to the elastic wave equation (Milana et al., 2014; Nazarian et al., 1988, 1983; Xia et al., 2004, 2002) or global optimization methods including genetic algorithms (Dong et al., 2014; Feng et al., 2005), and 2) full waveform inversion (Groos et al., 2014; Solano et al., 2014). Semi-analytical solutions can be used to robustly and efficiently invert for a 1D S-wave velocity model, but they become less accurate with increasing lateral heterogeneity in the subsurface. Global optimization methods can be used for a layered medium in practice, but the computation cost is not acceptable for 2D and 3D models with strong lateral variations in S-wave velocity. In contrast, waveform inversion estimates the velocity model that minimizes the misfit between the predicted and recorded data. However, the data-misfit function can be very sensitive to the accurate prediction of amplitudes, which is difficult to achieve with modeling methods that do not fully take into account viscoelastic and anisotropic effects. Moreover, a poor starting model will promote cycle skipping and convergence to a local minimum (Virieux and Operto, 2009).

To mitigate these problems, other types of data can be inverted that can be more accurately modeled and might enjoy a more quasi-linear relationship between the model and the data. For example, the traveltime misfit function is much less bumpy than the waveform misfit function. Hence, we can think of the less complex traveltimes as data *skeletonized* from the more complicated seismograms. The strategy of Luo and Schuster (1991a,b) is to invert the skeletonized data to get near the global minimum with no cycle skipping. Once the inverted model is close to the global minimum, an inversion method such as waveform inversion is used to reconstruct the final model.

We now adapt the skeletonized inversion strategy for inverting the dispersion curves of Rayleigh waves. Instead of picking traveltimes we pick the dispersion curve of the fundamental mode in the frequency-wavenumber domain and invert it for the S-wave velocity model. Higher-order modes can also be picked and inverted as well. This procedure is denoted as skeletonized wave equation inversion because the elastic wave equation is used to invert the velocity model from the dispersion curves. It can also invert for 2D or 3D S-wave velocity models compared to the 1D layered model in standard surface-wave inversion (Park et al., 1998). Our method differs from the waveform inversion approach of Baumstein et al. (2011) and Solano et al. (2014) who invert all of the surface-wave events or their windowed portions for the near-surface velocity information. They attempt to explain most of the observed waveforms with predicted ones, and so there still exists the possibility of getting stuck in a local minimum with a poor starting model. This is less of a problem

* Corresponding author.

http://dx.doi.org/10.1016/j.jappgeo.2016.07.019
0009-2541/© 2016 Elsevier B.V. All rights reserved.

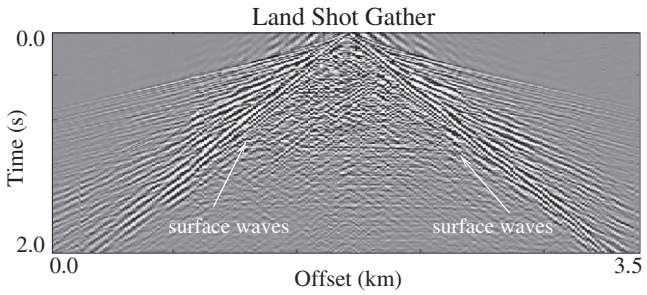

Fig. 1. Common shot gather recorded by a land survey.

with skeletonized inversion because it only attempts to explain the simple fundamental dispersion curve. However, if the medium is too complex then the fundamental dispersion curve cannot be easily identified and so skeletonized inversion might not be applicable.

This paper is divided into five sections. After the Introduction, the theory of skeletonized inversion of surface waves is described where the Fréchet derivative is estimated by a 1st-order difference approximation. The two terms in the difference approximation to the Fréchet derivative are computed by finite-difference solutions to the multidimensional elastic wave equation. We also provide the general workflow for inversion of skeletonized surface waves. In the third section, we first test skeletonized 1D and 2D inversion on synthetic data, then apply 1D inversion to field data to analyze the effectiveness and limitations of our method. The last section presents the summary of our work.

2. Theory

We now present the theory for skeletonized inversion of dispersion curves for multidimensional S-wave velocity models. In Fig. 1, there are many surface-wave cycles in the traces and so the waveform-misfit function for these data are highly nonlinear with respect to changes in the S-wave velocities. Therefore we should look for a means to simplify the data. One such reduction is to estimate the dispersion velocity $C(\omega)^{obs} = \omega/k(\omega)$ curve for the fundamental mode of Rayleigh waves in Fig. 2b, and invert it for the shear-velocity distribution. The locus of points for the fundamental mode is often identified by the maximum spectral amplitudes (Dong et al., 2014; Gabriels et al., 1987; Jianghai et al., 1999; Park et al., 1998) with the closest proximity to the $C(\omega)$ (or wavenumber) axis in Fig. 2.

A skeletonized surface-wave inversion algorithm that employs finite-difference solutions to the multidimensional elastic wave equation and an iterative gradient optimization algorithm is now presented. We call this method wave equation dispersion (WD) inversion because it inverts the dispersion curves associated with surface waves. The assumption is that dispersion curve of the fundamental dispersion velocity $C(\omega)$ has been picked, with the understanding that higher order modes can also be picked and inverted.

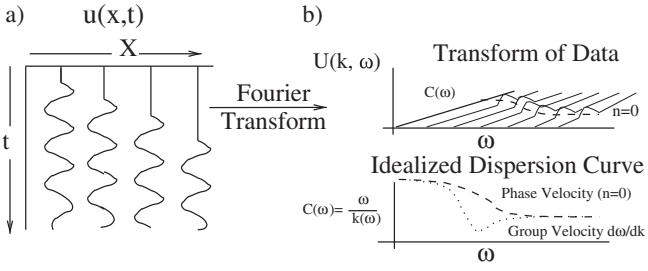

Fig. 2. Common shot gather on the left and right figures depict the (top right) actual $C(\omega) - \omega$ spectrum of the data and (bottom right) idealized dispersion curve for the fundamental Rayleigh mode for a two-layered elastic medium with a free surface. Here the dispersion velocity is $C(\omega) = \omega/k(\omega)$.

1. Form the misfit function ϵ

$$\epsilon = \frac{1}{2}\sum_{\omega}\left(C(\omega) - C(\omega)^{obs}\right)^2 + \frac{1}{2}R(c(\mathbf{x}))^2, \tag{1}$$

where $R(c(\mathbf{x}))$ is the regularization term, $c(\mathbf{x})$ is the S-wave velocity model, and $C(\omega)^{obs}$ describes the phase-velocity curve for the observed fundamental mode. Here, $C(\omega)$ is the fundamental phase-velocity predicted by solving the wave equation in the space-time domain and Fourier transforming a shot gather into the $\omega - k$ domain. This predicted curve is determined by manual picking or an automatic method that identifies the maximum amplitudes that are closest to the k axis to get $k(\omega)^{obs}$. The formula $C(\omega)^{obs} = \omega/k(\omega)^{obs}$ is used to get the phase-velocity curve. In Eq. (1), the roughness regularization term $R(c(\mathbf{x})) = \frac{dc(\mathbf{x})}{dz}$ penalizes sharp jumps in the S-wave velocity model. There are other methods for extracting the dispersion curve, such as the slowness-frequency transform of McMechan and Yedlin (1981) or the F-K method of Park et al. (1998). Fig. 3 shows the convex property of a desirable objective function so that an iterative gradient method will converge to the global minimum regardless of the starting model.

2. The steepest descent formula

$$\begin{aligned} c(\mathbf{x})^{(k+1)} &= c(\mathbf{x})^{(k)} - \alpha\gamma(\mathbf{x}), \\ &= c(\mathbf{x})^{(k)} - \alpha\sum_{\omega}\Delta C(\omega)^{(k)}\frac{\partial C(\omega)}{\partial c(\mathbf{x})} - \beta\frac{\partial R(\mathbf{x})}{\partial c(\mathbf{x})}, \end{aligned} \tag{2}$$

is used for reconstructing the S-wave velocity profile $c(\mathbf{x})$, where the regularization damping parameter is β. Here, the data residual is defined as $\Delta C(\omega)^{(k)} = C(\omega) - C(\omega)^{obs}$ where $C(\omega)$ is the predicted phase-velocity for the fundamental mode in a shot gather. In practice, we recommend the preconditioned conjugate gradient method in Luo and Schuster (1991a).

3. For an N-layer medium, there are $N + 1$ unknown S-velocity values so that the Fréchet derivative $\frac{\partial C(\omega)}{\partial c(\mathbf{x})}$ can be computed by the 1st-order finite-difference formula:

$$\frac{\partial C(\omega)}{\partial c_i(\mathbf{x})} \approx \frac{C(\omega)_{c(\mathbf{x})+\delta c_i(\mathbf{x})} - C(\omega)_{c(\mathbf{x})}}{\delta c_i(\mathbf{x})}, \tag{3}$$

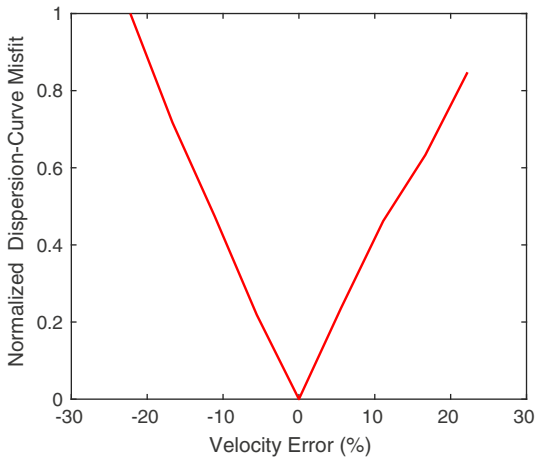

Fig. 3. Dispersion-curve misfit function versus S-wave velocity errors for a two-layer model. For this example there is no problem with getting stuck in a local minimum.

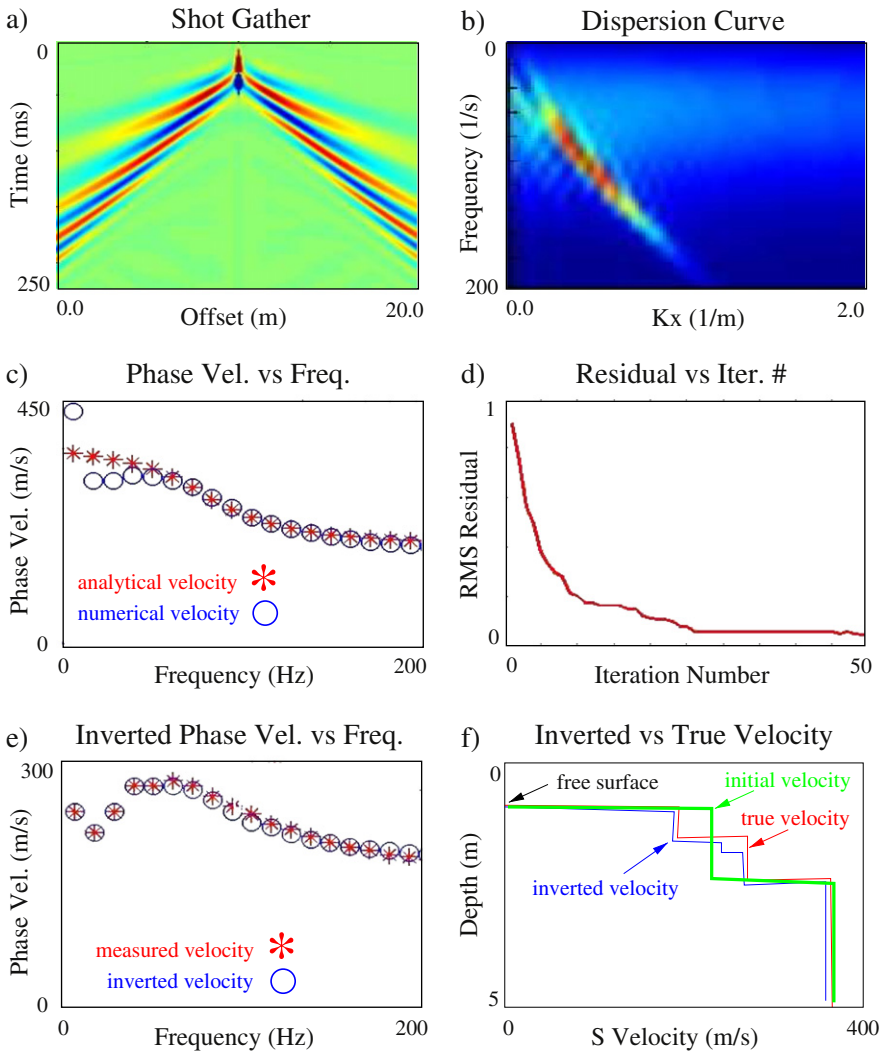

Fig. 4. Surface-wave inversion results for synthetic data. a) CSG for the vertical particle-velocity traces $u(g,t)$, b) its Fourier transform $U(k,\omega)$, c) the analytical (red) and numerically estimated (blue) phase-velocity $C(\omega)$ values for the fundamental-mode in a 2-layer medium, d) normalized residual vs iteration number for inverting phase velocities computed for the 3-layer model in f), e) inverted (blue) and measured (red) phase velocity points for the 3-layer model in f), and f) inverted S-wave velocity model denoted by blue lines. The true model denoted by the red line in f) consists of three layers below a free surface.

where $c(\mathbf{x})$ represents the reference S-wave velocity model and $\delta c_i(\mathbf{x})$ is the perturbed velocity in the ith layer. Two finite-difference simulations are required to compute $\frac{\partial C(\omega)}{\partial c_i(\mathbf{x})}$ in Eq. (3), one for the reference S-wave velocity model and one for the reference model with the S-wave velocity in the ith layer perturbed by $\delta c_i(\mathbf{x})$. The shot gathers from these two simulations in the space-time domain are FK transformed to get the two dispersion spectra, the fundamental dispersion curves are identified to get $k(\omega)_{c(\mathbf{x})}$ and $k(\omega)_{c(\mathbf{x})+\delta c_i(\mathbf{x})}$, and these dispersion curves are used to get the phase velocity curves $C(\omega)_{c(\mathbf{x})}$ and $C(\omega)_{c(\mathbf{x})+\delta c_i(\mathbf{x})}$. These phase velocities are then inserted into Eq. (3) to get the approximation to the Fréchet derivative. The normalized residual curve $\Delta C(\omega)^{(k)}$ is also computed and Eq. (2) is used to update the S velocity. The fundamental mode is largely insensitive to the P-velocity and density variations (Aki and Richards, 1980), so their values are not iteratively updated. For an $N-1$ layer velocity model, only $N+1$ finite-difference (FD) simulations are computed for one shot at each iteration. For convenience, we assume a constant density and assign the P-wave velocity V_p to be proportional to the S-wave velocity model. If the model is 2D, then the number of FD simulations/iteration will increase by the number of unknowns per layer.

3. The workflow for this method

In summary, our proposed skeletonized inversion includes the following steps:

1. 2D Fourier transform of the observed data and generate the dispersion curve.
2. Estimate the initial velocity model from the dispersion curves.
3. Split the initial model into finer layers and perturb each of them with a small value to calculate the Fréchet derivative. The details for implementing WD inversion for a 2D medium are discussed in the next section.

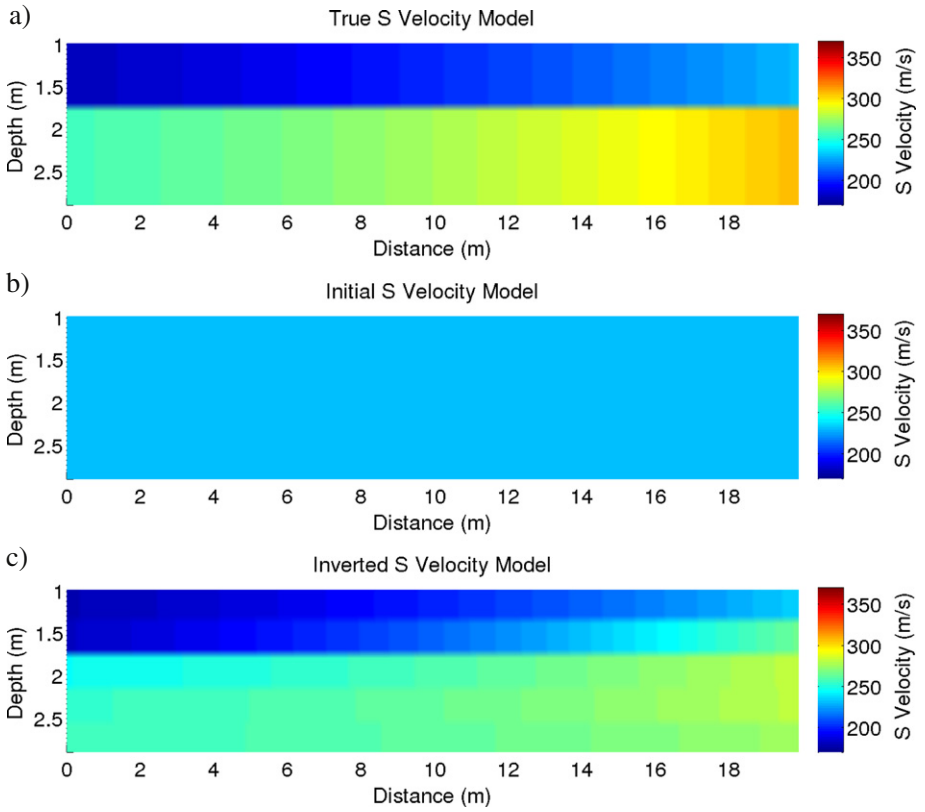

Fig. 5. 2D inversion results. a) True S-wave velocity model, b) initial S-wave velocity model which is a constant velocity model and c) inverted S-wave velocity model.

4. For the current model, compute the synthetic data, the Fréchet derivative, the residual, and the misfit gradient.
5. Update the current model using the steepest descent method.
6. Repeat steps 3–5 until the inverted results are acceptable.

For 2D inversion, two more parameters need to be inverted under the quadratic assumption for laterally varying velocities. We recommend the hierarchy method (Brossier et al., 2009; Operto et al., 2013; Prieux et al., 2013) to retrieve different parameter classes

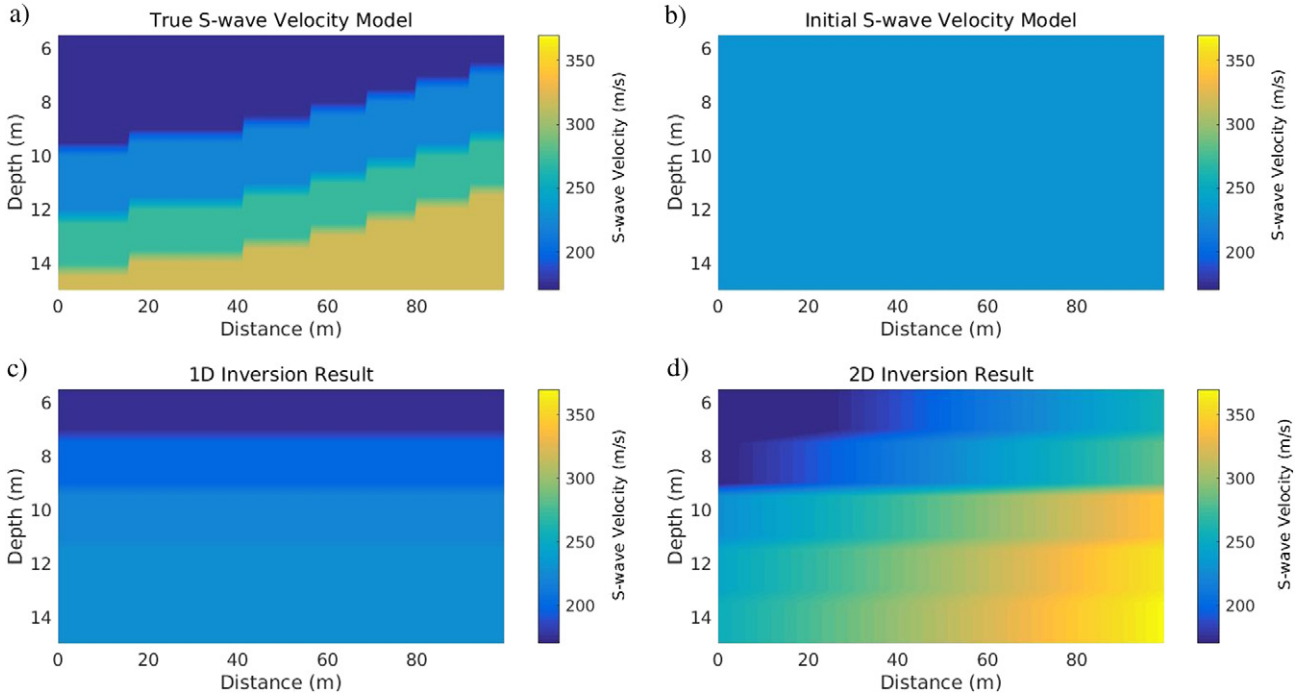

Fig. 6. 2D inversion results. a) True S-wave velocity model, b) initial S-wave velocity model which is a constant velocity model, c) inverted S-wave velocity model using the 1D method and d) inverted S-wave velocity model using the 2D method.

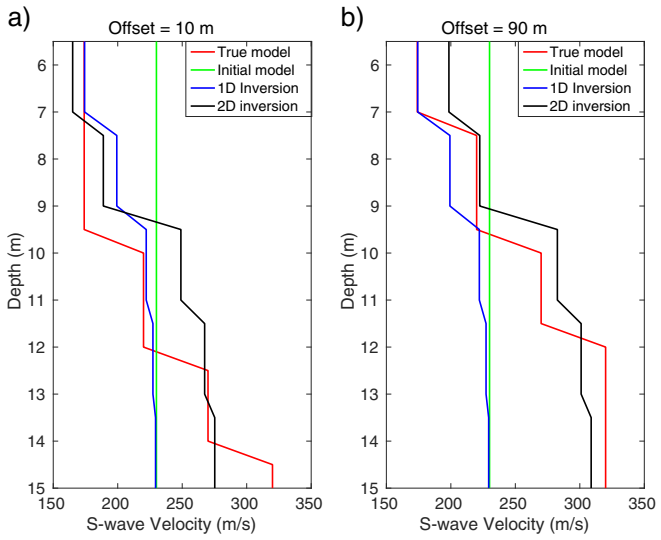

Fig. 7. True and inverted S-wave velocity profiles at a) x = 10 m and b) x = 90 m.

successively. To be more specific, we implement 1D inversion for the first several iterations and then invert for the 1D model and lateral variations simultaneously.

4. Numerical examples

The skeletonized inversion method is first tested on synthetic data and then applied to field data.

4.1. 1D inversion of synthetic data

An example of inverting for the S-wave velocity distribution by skeletonized surface-wave inversion is now presented. A shot gather is computed by a finite-difference solution to the 2D elastic wave equation and is shown in Fig. 4a for the 3-layer model in Fig. 4f (red line). Here, the traces are the vertical-component particle-velocity measurements on the free surface. The source is simulated as an explosive point source in the 2D modeling code, where the source wavelet is a Ricker wavelet peaked at 80 Hz. This means that the effective source bandwidth is between 60 Hz and 200 Hz. An FK transform is applied to the shot gather to give the spectrum shown in Fig. 4b, which is then transformed into the phase-velocity spectrum depicted in Fig. 4c. The blue dots correspond to the measured curve and the red dots represent the actual phase-velocity curve. The paucity of low-frequency information and long-offset traces prevented an accurate estimate of the phase velocities at low frequencies.

The model is discretized into 5 homogeneous layers with the same thickness and each layer having an unknown S-wave velocity. The steepest descent algorithm after 50 iterations gives the phase-velocity curve in Fig. 4e and the blue S-wave velocity profile in Fig. 4f. It is obvious that the inverted S-wave velocity model closely agrees with the actual one.

4.2. Extension to a 2D medium

The skeletonized inversion procedure can be extended to models with lateral heterogeneity in the S-wave velocity by assuming a quadratic velocity variation $c(x)_i$ in the ith layer:

$$c(x)_i = c_i + \gamma_i x + \zeta_i x^2, \tag{4}$$

where c_i, γ_i and ζ_i are unknown constants that are to be inverted for by the steepest descent formula (2). Instead of inverting for just one unknown in each layer, three unknowns are to be inverted which triples the computational cost. However, the total computational cost is quite affordable for velocity profiles with no more than several dozen layers. As an example, Fig. 5 depicts the actual and predicted lateral velocity variations using the steepest descent method to invert for γ_i and ζ_i in each layer for 3 shot gathers. The lateral velocity variations are acceptably reconstructed as shown in Fig. 5. The velocity gradient in the shallowest layer is most accurately reconstructed, as one might expect for this data where the lowest frequency is only 60 Hz. Surface waves are typically sensitive only to velocity variations down to a depth of about 1/3 of a wavelength.

We also compared the perfomances of the 1D and 2D inversion methods on the more complicated S-wave velocity model shown in Fig. 6a. The lateral velocity variations are not restricted to one layer and there are 3 shots separated by 8.5 m and each shot shoots into the same 200 receivers/shot spaced at a 0.5 m receiver interval. The dominant frequency of the source is 20 Hz to allow the surface wave to penetrate to the deepest part of the model. We calculate the Fréchet derivatives and misfit functions for each shot and then stack the misfit gradients for different shots to get the total misfit gradient for all the data. The initial velocity model is the constant velocity model shown in Fig. 6b, and both the 1D and 2D inversion results are shown in Fig. 6c and d respectively. For a more precise comparison, we plot the S-wave velocities versus depth at the offsets of 10 m and 90 m in Fig. 7a and b, respectively. It is obvious that the tomogram computed from the 2D WD method is more accurate than the one computed by the 1D WD method. We use the hierarchy inversion strategy to eliminate the variable influence of different parameters in our objective function. As shown in Fig. 8, the normalized data residual decreases in two stages, the monoparameter inversion stage (blue arrow) and the multiparameter inversion stage (green arrow).

4.3. 1D inversion of field data

A seismic land survey was carried out near the Red Sea coast in Saudi Arabia to give the recorded shot gather in Fig. 9a. The geophone spacing is 5 m, the source is a hammer on a metal plate, and the dominant frequency in the traces is about 40 Hz. An FK transform is applied to the Fig. 9a shot gather and the phase-velocity curve for the fundamental-mode is picked and displayed as the red dots

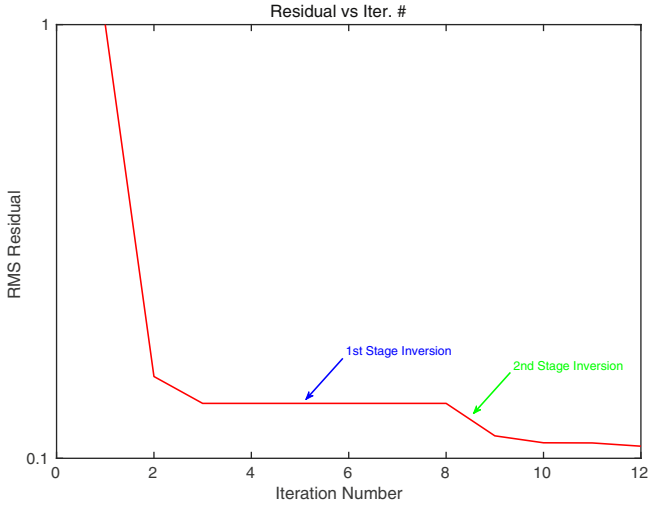

Fig. 8. Normalized data residual versus number of iterations. Only c_i in Eq. (4) is inverted in the first stage (see blue arrow) of iterations, and then both γ_i and ζ_i are inverted (see green arrow) at the later iterations.

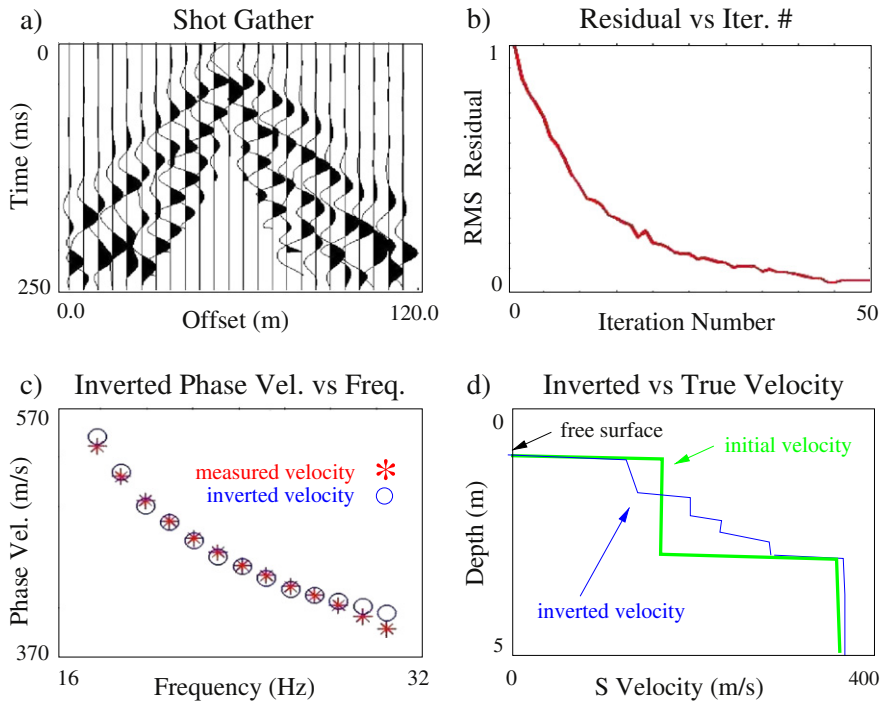

Fig. 9. Surface wave inversion results for data recorded by a land survey near the Red Sea. a) CSG for the vertical particle velocity traces, b) residual vs iteration number, c) measured (red) and inverted (blue) phase-velocity values $C(\omega)$ for the fundamental mode, and d) inverted S-wave velocity model (blue curve).

in Fig. 9c. Using a 5-layer velocity model, these phase velocities are inverted using the steepest descent formula in Eq. (2) to give the predicted blue points in Fig. 9c. The P-wave velocity values were extracted from a P-wave velocity tomogram, and a constant density model is assumed. Fig. 9d shows the initial velocity model depicted by the green curve and the inverted S-wave velocity profile shown in Fig. 9d provides a reasonable range of S velocities for these types of sediments.

To evaluate the uncertainty of our inversion result, a sensitivity matrix is computed to assess the sensitivity of the data to changes in the S-wave velocity model. The elements of the sensitivity matrix are the computed Fréchet derivatives $Aij = \frac{\partial C(\omega_j)_i}{\partial c_i}$ for different frequencies and layer numbers. As an example, Fig. 10 plots these values for the 5-layer model in Fig. 9d and shows that for the available frequency band, the dispersion curve is most sensitive (i.e., hotter colors) to the velocity variations to a depth of about 3 m. Thus, these are the layers which should provide the least uncertainty in velocity reconstruction.

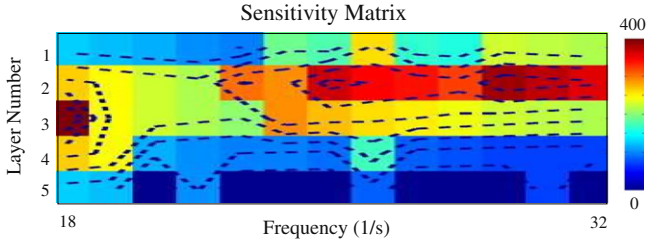

Fig. 10. Sensitivity matrix of Fréchet derivative values for the 5-layer model in Fig. 9d. As expected, higher frequencies in the data are mainly influenced by the S-velocities in shallow layers.

5. Conclusions

We presented a wave-equation method for inverting the dispersion curves associated with surface waves. The main benefits of this approach are that it mitigates cycle skipping problems associated FWI of surface waves, it is efficient for a limited number of layers, and is applicable to 2D and 3D velocity models. It is easily extended to higher-order modes and dispersion curves for Love waves. In our examples, the dispersion curve for the fundamental mode is automatically picked and inverted by a steepest descent method in conjunction with finite-difference solutions to the elastic wave equation. Higher-order modes can also be picked and inverted. Results for both synthetic data and field data verify the effectiveness of this method and reveal some of its limitations.

The 2D inversion example demonstrates that our inversion result can reconstruct the horizontal variations of the S-wave velocities as long as there is sufficient smoothness in the velocity model, a sufficient number of shot gathers with wide aperture recording, and a wide enough bandwidth in the source wavelet. The proposed method has a good vertical resolution if the velocity increases with depth.

A limitation of this method is that the computational cost becomes prohibitive if there are a large number of unknown parameters because each one requires a FD solution of the elastic wave equation. To overcome this expense, Li and Schuster (Accepted) developed the analytic formulas for implementing skeletonized surface wave inversion with the adjoint state method.

Acknowledgments

We thank KAUST and CSIM sponsors for their support. Zhang and Liu thank Tariq Alkhalifah for his help. We thank three reviewers for their valuable comments and suggestions. The research was

partly funded by the National Nature Science Foundation of China (Grant No. 41430321).

References

Aki, K., Richards, P., 1980. Quantitative Seismology. W. H. Freeman and Company, San Francisco.

Baumstein, A., Ross, W., Lee, S., 2011. Simultaneous source elastic inversion of surface waves. 73rd EAGE Conference and Exhibition.

Brossier, R., Operto, S., Virieux, J., et al. 2009. Two-dimensional seismic imaging of the valhall model from synthetic OBC data by frequency domain elastic full-waveform inversion. 2009 SEG Annual Meeting.

Dong, Z., Xiaofei, C., Xiaogui, M., 2014. Rayleigh wave analysis and inversion for near surface shear wave velocity model building. Beijing 2014 International Geophysical Conference and Exposition. pp. 1217–1220.

Feng, S., Sugiyama, T., Yamanaka, H., 2005. Effectiveness of multi-mode surface wave inversion in shallow engineering site investigations. Explor. Geophys. 36 (1), 26–33.

Gabriels, P., Snieder, R., Nolet, G., 1987. In situ measurements of shear-wave velocity in sediments with higher-mode Rayleigh waves. Geophys. Prospect. 35 (2), 187–196.

Groos, L., Schäfer, M., Forbriger, T., Bohlen, T., 2014. The role of attenuation in 2d full-waveform inversion of shallow-seismic body and Rayleigh waves. Geophysics 79 (6), R247–R261.

Jianghai, X., Miller, R.D., Park, C.B., 1999. Estimation of near-surface shear-wave velocity by inversion of Rayleigh waves. Geophysics 64 (3), 691–700.

Li, J., Schuster, G.T., 2016. Wave equation dispersion inversion. Geophys. J. Int. (Accepted).

Luo, Y., Schuster, G.T., 1991. Wave equation inversion of skeletalized geophysical data. Geophys. J. Int. 105 (2), 289–294.

Luo, Y., Schuster, G.T., 1991. Wave-equation traveltime inversion. Geophysics 56 (5), 645–653.

McMechan, G.A., Yedlin, M.J., 1981. Analysis of dispersive waves by wave field transformation. Geophysics 46 (6), 869–874.

Milana, G., Bordoni, P., Cara, F., Di Giulio, G., Hailemikael, S., Rovelli, A., 2014. 1d velocity structure of the Po river plain (Northern Italy) assessed by combining strong motion and ambient noise data. Bull. Earthq. Eng. 12 (5), 2195–2209.

Nazarian, S., Stokoe, I., Kenneth, H., Briggs, R.C., Rogers, R., 1988. Determination of pavement layer thicknesses and moduli by SASW method. Transp. Res. Rec. (1196).

Nazarian, S., Stokoe, I., Kenneth, H., Hudson, W., 1983. Use of Spectral Analysis of Surface Waves Method for Determination of Moduli and Thicknesses of Pavement Systems. , pp. 930.

Operto, S., Gholami, Y., Prieux, V., Ribodetti, A., Brossier, R., Metivier, L., Virieux, J., 2013. A guided tour of multiparameter full-waveform inversion with multicomponent data: from theory to practice. Lead. Edge 32 (9), 1040–1054.

Park, C.B., Miller, R.D., Xia, J., 1998. Imaging dispersion curves of surface waves on multi-channel record. SEG Expanded Abstr. 17 (1), 1377–1380.

Prieux, V., Brossier, R., Operto, S., Virieux, J., 2013. Multiparameter full waveform inversion of multicomponent ocean-bottom-cable data from the valhall field. Part 1: imaging compressional wave speed, density and attenuation. Geophys. J. Int. Ggt177.

Solano, P., Donno, C.D., Chauris, H., 2014. Alternative waveform inversion for surface wave analysis in 2-D media. Geophys. J. Int. 198 (3), 1359–1372.

Virieux, J., Operto, S., 2009. An overview of full-waveform inversion in exploration. Geophysics 74 (6), WCC1–WCC26.

Xia, J., Miller, R.D., Park, C.B., Ivanov, J., Tian, G., Chen, C., 2004. Utilization of high-frequency rayleigh waves in near-surface geophysics. Lead. Edge 23 (8), 753–759.

Xia, J., Miller, R.D., Park, C.B., Tian, G., 2002. Determining q of near-surface materials from Rayleigh waves. J. Appl. Geophys. 51 (2), 121–129.